A Protocol for the Interpretation of Side-Chain Dynamics Based on NMR Relaxation: Application to Phenylalanines in Antamanide

T. Bremi, R. Brüschweiler,* and R. R. Ernst*

Contribution from the Laboratorium für Physikalische Chemie, ETH Zentrum, 8092 Zürich, Switzerland

Received October 18, 1996[⊗]

Abstract: A new protocol for the interpretation of NMR relaxation data in terms of intramolecular motion is described. At first, a long molecular dynamics simulation of the system is generated and analyzed with respect to nuclear spin relaxation-active motional modes. In a second step, an analytical model is conceived on the basis of the computational results. Finally, the model parameters are determined numerically by a least-squares fit to the experimental NMR data. This protocol was applied to the phenylalanine side-chain dynamics in the cyclic decapeptide antamanide. A 100 ns Langevin dynamics simulation was analyzed in terms of dihedral angle fluctuations, correlation functions, and potentials of mean force. For χ_1 and χ_2, motion in a harmonic potential is observed which is interrupted by occasional jumps between different rotamers over relatively high barriers. This behavior leads to an analytical Gaussian axial fluctuation and jump model, which is an extension of the previously proposed GAF model (Brüschweiler, R.; Wright, P. E. *J. Am. Chem. Soc.* **1994**, *116*, 8426).

1. Introduction

It is nowadays widely recognized that the detailed knowledge of the average structure of a biomolecule, as it can be determined by X-ray crystallography or nuclear magnetic resonance (NMR) spectroscopy, is insufficient for the understanding of its chemical reactivity and its molecular interactions. Biomolecular function is intimately connected to molecular flexibility, and structural data must be supplemented by information on intramolecular dynamics and mobility.

NMR is a most powerful and versatile tool for the study of molecular dynamics.[1−3] In particular, nuclear spin relaxation measurements can provide a wealth of detailed information on intramolecular mobility. ^{15}N relaxation measurements have become a standard method for the investigation of the backbone dynamics of proteins,[4] and ^{13}C relaxation is well-suited for studying the functionally important amino acid side-chain dynamics.

The design of appropriate motional models for the interpretation of the relaxation measurements has been a central issue from the very beginning, realizing that the available measurements are invariably insufficient for a self-contained description of molecular dynamics. According to Bloch−Wangsness−Redfield relaxation theory,[5,6] the experimentally accessible information is contained in the power spectral density function which is the Fourier transform of the correlation function of the time-dependent lattice parts of the relaxation-active spin interactions. Since the pioneering work of Woessner,[7] who considered free diffusion and jump motion of an internuclear vector about a single axis, much effort has been directed toward the development of improved models. Wallach extended the model, taking into account free rotations and jump motions about adjacent chemical bonds along a side chain.[8] In subsequent work, the model was modified to allow for jump motions between different rotamers and restricted rotational diffusion within a rotameric state represented by a square-well potential,[9,10] or diffusion within a cone ("wobbling in a cone").[11,12]

In the early 1980s, two important complementary developments began. On the one hand, Lipari and Szabo[13] addressed the problem that experimental relaxation data often do not allow one to discriminate between different motional models. They introduced a "model-free" description, where internal motion is locally parametrized by an order parameter and an intramolecular correlation time, thereby preventing a possible overinterpretation of the data. An extension of this concept has been described in ref 14. In the model-free formalism, one refrains from a physical preconception and analyzes the experimental data in terms of mathematical correlation functions which themselves are parametrized by a minimum set of timescale and order parameters. Such a local description of motion does not yield immediate information about correlated dynamics or long-range motions.[15] The connection to a physical model is thereby lost, and the link has to be established in a second interpretative step. The relation between the model-free description and the restricted rotational diffusion plus jump model for aromatic side chains[9,10] has been derived by Levy and

[⊗] Abstract published in *Advance ACS Abstracts,* April 1, 1997.

(1) Abragam, A. *Principles of Nuclear Magnetism*; Clarendon Press: Oxford, 1961.
(2) Ernst, R. R.; Bodenhausen, G.; Wokaun, A. *Principles of Nuclear Magnetic Resonance in One and Two Dimensions*; Clarendon Press: Oxford, 1987.
(3) Tycko, R., Ed. *NMR Probes of Molecular Dynamics*; Kluwer: Dordrecht, The Netherlands, 1994.
(4) Wagner, G. *Curr. Opin. Struct. Biol.* **1993**, *3*, 748−754.
(5) (a) Wangsness, R. K.; Bloch, F. *Phys Rev.* **1953**, *89*, 728−739. (b) Bloch, F. *Phys. Rev.* **1956**, 102, 104−135.
(6) (a) Redfield, A. G. *IBM J. Res. Dev.* **1957**, *1*, 19−31. (b) Redfield, A. G. *Adv. Magn. Reson.* **1965**, *1*, 1−32.
(7) Woessner, D. E. *J. Chem. Phys.* **1962**, *36*, 1−4.
(8) Wallach, D. *J. Chem. Phys.* **1967**, *47*, 5258−5268.
(9) Wittebort, R. J.; Szabo, A. *J. Chem. Phys.* **1978**, *69*, 1722−1736.
(10) London, R. E.; Avitabile, J. *J. Am. Chem. Soc.* **1978**, *99*, 7159−7165.
(11) Kinosita, K., Jr.; Kawato, S.; Ikegami, A. *Biophys. J.* **1977**, *20*, 289−305.
(12) Lipari, G.; Szabo, A. *Biophys. J.* **1980**, *30*, 489−304.
(13) Lipari, G.; Szabo, A. *J. Am. Chem. Soc.* **1982**, *104*, 4546−4559, 4559−4570.
(14) Clore, G. M.; Szabo, A.; Bax, A.; Kay, L. E.; Driscoll, P. C.; Gronenborn, A. M. *J. Am. Chem. Soc.* **1990**, *112*, 4989−4991.
(15) Brüschweiler, R. *J. Chem. Phys.* **1994**, *102*, 3396−3403.

S0002-7863(96)03650-5 CCC: $14.00

Sheridan.[16] A concept, which is related to the model-free approach, has been proposed and applied by Peng and Wagner[17,18] aiming at a direct determination of power spectral density components at various frequencies. As in the model-free formalism, the physical interpretation of the power spectral densities has to follow in a subsequent step.

A different approach has been pursued by Levy, Wolynes, and Karplus[19] who calculated for the first time NMR relaxation parameters on the basis of molecular dynamics (MD) simulations. The trajectories allowed them to estimate the accuracy of the inherent assumptions in the analytical models, such as the independence of rotations about different side-chain axes. It was attempted to overcome the insufficient sensitivity of the relaxation data for discerning different analytical models by introducing independent knowledge in form of empirical molecular force fields. More recently, it has been shown that normal mode analysis of proteins is applicable for the interpretation of fast-time-scale dynamical effects on NMR relaxation.[20−22]

To assess the pros and cons of different approaches, it is useful to define evaluation criteria. In our opinion, an ideal model should fulfill three criteria: (I) It should be *realistic* and take into account our knowledge on feasible molecular dynamics modes. (II) It should allow an *accurate* explanation of the experimental data within the experimental errors. (III) It should be *simple* and involve a minimal number of motional parameters.

The most realistic description of intramolecular dynamics today is by an analytical force field, allowing for molecular dynamics simulations mimicking the natural processes. One may conceive to adjust the force field parameters on the basis of the NMR data in the hope of obtaining a more realistic and reliable potential energy surface. This procedure is unfortunately seldom feasible as the number of force field parameters involved is normally high and surmounts the number of available measurements. For quasi-harmonic dynamics, in the absence of jump processes, a collective motional model has been introduced recently, where NMR relaxation data are fitted by adjusting amplitudes and directions of collective normal modes.[23]

The application of an analytical model requires restrictive assumptions to be made about the NMR-relevant motional modes, such as small-amplitude local fluctuations or specific jump or diffusion-type processes. In this way, an interpretation of NMR data becomes feasible, but will remain highly dependent on the model assumptions. Often several alternatives can hardly be distinguished on the basis of the available data alone.[13]

The protocol presented in this work, which is outlined in Figure 1, combines positive features of the different approaches. It advocates an analytical model that is based on an MD simulation rather than obtained by physical intuition, circumventing some of the arbitrariness involved in selecting a motional model on other grounds. The protocol was tested on the phenylalanine side-chain dynamics in the cyclic decapeptide antamanide (Figure 2), and compared with an NMR study[24] where experimental data are interpreted in terms of rotational motions about χ_1 and χ_2. From the analysis of a 100 ns

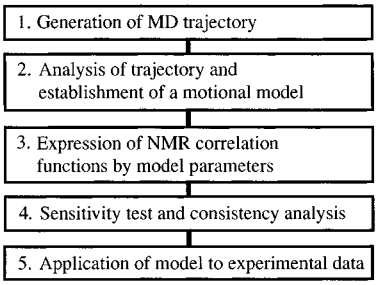

Figure 1. Outline of the proposed procedure.

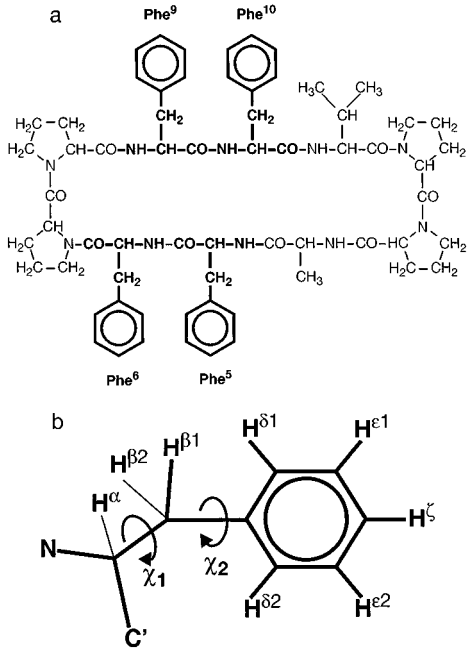

Figure 2. (a) Cyclic decapeptide antamanide and (b) the phenylalanine residue with atom definitions used in the text.

Langevin dynamics simulation of antamanide, the motional picture emerging for the phenylalanine side chains consists of strongly damped harmonic oscillations within the localized potential wells, interrupted by occasional jumps between different rotameric states over relatively high barriers. The presented motional model can be considered as an extension of the Gaussian axial fluctuation (GAF) model[25] to 2 degrees of freedom superimposed by lattice jump motion, called the GAF & jump model. Mathematical details of the model are described in the Appendix. Relations between harmonic motions and correlation functions[26] have been used previously also in the context of fluorescence anisotropy decay theory.[27,28]

2. Interpretation of NMR Relaxation Data by a Physical Model Derived from MD Simulations

The proposed analysis procedure consists of five steps (Figure 1):

(1) Molecular Dynamics Simulation. At first, an MD simulation trajectory of the system under investigation is generated to identify relevant dynamical modes. The success of the approach depends crucially on the choice of a reliable and well-tested force field which faithfully represents the actual molecular properties. The MD simulation should ideally span at least 10 times the largest internal motional correlation time, but does

(16) Levy, R. M.; Sheridan, R. P. *Biophys. J.* **1983**, *41*, 217−221.
(17) Peng J. W.; Wagner G. *J. Magn. Reson.* **1992**, *98*, 308−332.
(18) Peng J. W.; Wagner G. *Biochemistry* **1992**, *31*, 8571−8586 .
(19) Levy, R. M.; Karplus, M.; Wolynes, P. G. *J. Am. Chem. Soc.* **1981**, *103*, 5998−6011.
(20) Brüschweiler, R. *J. Am. Chem. Soc.* **1992**, *114*, 5341−5344.
(21) Palmer, A. G.; Case, D. A. *J. Am. Chem. Soc.* **1992**, *114*, 9059−9067.
(22) Sunada, S.; Gō, N.; Koehl, P. *J. Chem. Phys.* **1996**, *104*, 4768−4775.
(23) Brüschweiler, R.; Case, D. A. *Phys. Rev. Lett.* **1994**, *72*, 940−943.
(24) Bremi, T.; Ernst, M.; Ernst, R. R. *J. Phys. Chem.* **1994**, *98*, 9322−9334.
(25) Brüschweiler, R.; Wright, P. E. *J. Am. Chem. Soc.* **1994**, *116*, 8426−8427.
(26) Chandrasekhar, S. *Rev. Mod. Phys.* **1943**, *15*, 1−89.
(27) Kinosita, K., Jr.; Ikegami, A. *Biophys. J.* **1982**, *37*, 461−464 .
(28) Szabo, A. *J. Chem. Phys.* **1984**, *81*, 150−167.

not need to be much longer than about 10 times the overall tumbling correlation time τ_c. For biomolecules simulation times of ten to hundreds of nanoseconds are usually necessary and appropriate, which precludes the full representation of the solvent interactions, and often Langevin dynamics must be employed. Obviously, a judiciously planned compromise between affordable computation time and acceptable statistical properties of the trajectory must be found. In the present context, good statistics is mandatory to test whether the analytical model derived from the simulation can quantitatively reproduce the NMR relaxation data calculated directly from the simulation.

It is mostly unrealistic to expect that the MD simulation would cover the entire ergodic ensemble of possible structures, in spite of the extensive computation time. It is thus necessary to start the simulation from a relevant molecular conformation, e.g., a high-resolution structure obtained by NMR or X-ray. In the presence of slow intramolecular dynamics modes in the micro- or milliseconds that cannot be covered by the MD simulation, several runs with properly selected initial structures should be performed and the resulting spectral density functions averaged.

(2) Analysis of the Trajectory and Construction of the Motional Model. Understanding the MD trajectory requires an analysis of the soft motional degrees of freedom, which often coincide with the mobile dihedral angles. By means of a statistical analysis, rotamer populations and their respective interconversion rates can be estimated. Computation of auto-correlation and cross-correlation functions of dihedral angles reveals the relevant motional time scales and the presence of correlation effects. Furthermore, evaluation of potentials of mean force[29,30] along soft motional degrees of freedom, leading to an effective free energy surface, may allow an analytical parametrization of the potential surface which is sufficiently realistic to reproduce qualitative and quantitative properties of the MD trajectory. An example of such an analysis is given in section 3.

For the sake of clarity, we sketch conceivable models that may result from this type of analysis for amino acid side-chain motions.

(i) Rotational diffusion model: A potential of mean force that is virtually flat within k_BT for a free or restricted angular range would suggest an unrestricted or restricted rotational diffusion model characterized by a rotational diffusion constant and possibly a rotational restriction angle.[7−10]

(ii) Gaussian axial fluctuation model: A locally quadratic potential of mean force, limited by high barriers, suggests a Gaussian axial fluctuation model, characterized by a variance σ_i^2 and an effective correlation time τ_i.[25−28]

(iii) Rotational jump model: A potential of mean force with several narrow minima, separated by barriers of intermediate height (several k_BT), suggests the application of a discrete rotational jump model[7] with equal or unequal site populations and a set of transfer rate constants.

(iv) Rotational fluctuation and jump model: A more general model combines either (i) and (iii) or (ii) and (iii). Local fluctuations in either a square well or quadratic potential are combined with jumps between different rotamers. The local fluctuations are again characterized by a variance σ_i^2, which may differ from rotamer to rotamer while the jump processes are governed by transfer rate constants.

(v) Wobbling in a cone: The significant presence of fast backbone dynamics may necessitate explicit parametrization of the motion of the $C^\alpha-C^\beta$ vector, for example, as diffusion inside a cone.[11,12]

In situations with two or more segmental motions, such as in the situation of phenylalanine side chains with a χ_1 and a χ_2 rotor, the different processes can also be correlated, requiring, for example, the use of correlation coefficients to characterize the combined motion.

(3) Analytical Expression of NMR Correlation Functions by Model Parameters. At this stage of the procedure, the link between the parametrized description of the observed MD motions and NMR relaxation is established. For this purpose, analytical expressions are derived for the relaxation-relevant correlation functions depending explicitly on the chosen model parameters. This step is described in some detail in the Appendix for the phenylalanine side chains.

(4) Sensitivity Analysis and Consistency Test. There is no *a priori* guarantee that NMR relaxation data allow an accurate and robust determination of the introduced model parameters. A sensitivity analysis and consistency test, described in section 4, is therefore necessary: NMR relaxation data are calculated on the basis of the correlation functions of the MD calculation, and the parameters of the model are fitted to these values. Agreement between the parameters determined in step 2 and the fitted parameters, and their sensitivity with respect to errors in the relaxation data, can thereby be assessed.

(5) Application to Experimental Data. A motional model that passes the consistency test is then ready for application to experimental relaxation data. The availability of other experimental data, such as scalar *J* coupling constants, may help to improve the accuracy of the determined model parameters. Finally, the extracted experimental motional parameters may be compared with the LD results. If the differences are reasonably small and at least qualitative agreement is found, the protocol is self-consistent. Larger differences, on the other hand, may suggest the examination of further motional models, e.g., extracted by using other force fields or other initial structures.

3. MD Simulation of Antamanide

3.1. Computational Details. A 100 ns Langevin dynamics (LD) simulation (stochastic dynamics) was performed for the cyclic decapeptide antamanide (Figure 2a) using the CHARMM program with the force-field parameters of version 22.[31,32] For the initial structure, the antamanide backbone structure (++), determined by the MEDUSA algorithm,[33] was chosen and the cyclic topology of antamanide was treated in an all-atom approach with explicit hydrogen atoms (total of 162 atoms). The SHAKE algorithm[34] was applied, and the integration step size was set to 1 fs. No cutoff was used for the nonbonded interactions. The dielectric permittivity was set to 1.0. Other detailed accounts of LD simulations of antamanide can be found in ref 35.

(29) Brooks, C. L., III; Karplus, M.; Pettitt, B. M. *Proteins: A Theoretical Perspective of Dynamics, Structure, and Thermodynamics*; John Wiley & Sons: New York, 1987.

(30) Beutler, T. C.; Bremi, T.; Ernst, R. R.; van Gunsteren, W. F. *J. Phys. Chem.* **1996**, 100, 2637−2645.

(31) Brooks, R. B.; Bruccoleri, R. E.; Olafson, B. D.; States, D. J.; Swaminathan, S.; Karplus, M. *J. Comput. Chem.* **1983**, *4*, 187−217.

(32) Mackerell, A. D. Jr.; Bashford, D.; Bellot, M.; Dunbrack, R. L.; Field, M. J.; Fischer, S.; Gao, J.; Guo, H.; Joseph, D.; Ha, S.; Kuchnir, L.; Kuczera, K.; Lau, F. T. K.; Mattos, C.; Michnick, S.; Nguyen, D. T.; Ngo, T.; Prodhom, B.; Roux, B.; Schlenkrich, B.; Smith, J.; Stote, R.; Straub, J.; Wiorkiewicz-Kuczera, J.; Karplus, M. *Biophys. J.* **1992**, *61*, A134.

(33) Brüschweiler, R.; Blackledge, M.; Ernst, R. R. *J. Biomol. NMR* **1991**, *1*, 3−11. (b) Blackledge, M. J.; Brüschweiler, R.; Griesinger, C.; Schmidt, J. M.; Xu, P.; Ernst, R. R. *Biochemistry* **1993**, *32*, 10960−10974.

(34) Ryckaert, J. P.; Cicotti, G.; Berendsen, H. J. C. *J. Comput. Phys.* **1977**, *23*, 327−341.

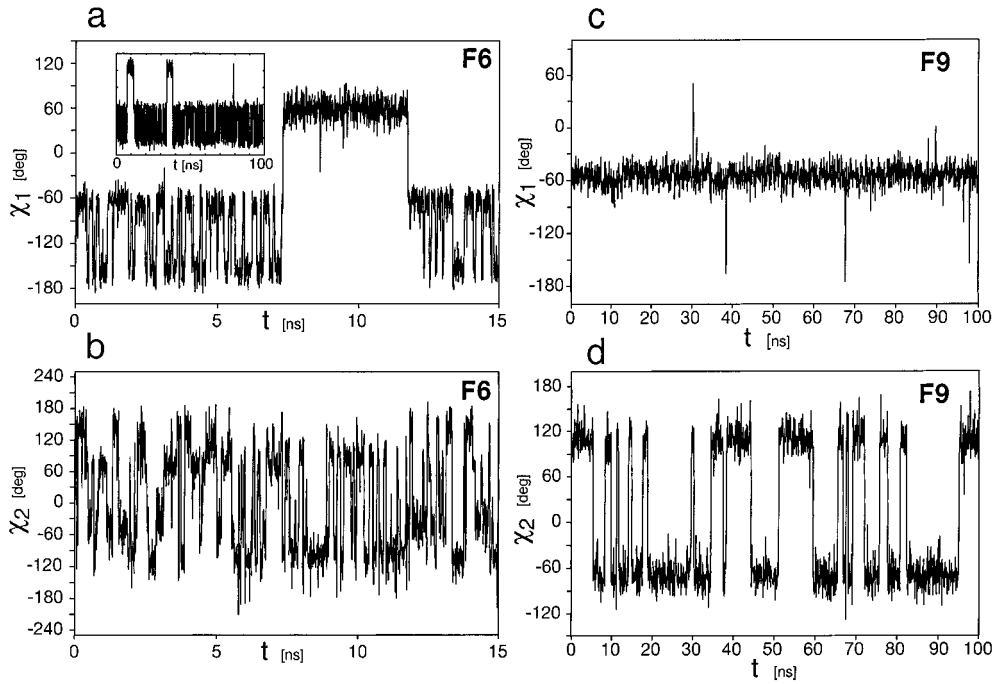

Figure 3. Dihedral angle trajectories of the two phenylalanine residues 6 and 9 of antamanide: (a) χ_1 trajectory of F6 (inset shows the full 100 ns trajectory); 387 transitions are observed from the conformer I ($\chi_1 = -60°$) to II ($\chi_1 = -180°$) and 387 transitions from II to I, 3 transitions from I to III ($\chi_1 = 60°$), and also 3 transitions from III to I; (b) χ_2 trajectory of F6; about 310 ring flips occur during the 100 ns trajectory (due to the χ_1, χ_2 jump correlation, the flip count is ambiguous); (c) χ_1 trajectory of F9; (d) χ_2 trajectory of F9; 20 ring flips are observed.

The simulation temperature was elevated to 400 K for more comprehensive sampling of the side-chain conformations. While such a procedure has the potential drawback that the sampled motion may no longer be representative for the experimental measurement conditions, for antamanide we have found that LD simulations carried out at 300 K[30,35] and a MD simulation in chloroform at 250 K[36] show motional behavior qualitatively similar to that observed in the present work. Since the primary purpose of the MD simulation in this protocol is the extraction of a qualitative rather than a quantitative dynamical picture, a moderate increase of the temperature is worth consideration. Rare backbone flips that would disturb the statistics were avoided by constraining all heavy backbone atoms by a weak harmonic potential of strength 0.1 kcal/Å^2. Obviously, the backbone conformation may affect the side-chain mobility, but the qualitative motional models, which shall be deduced, are not altered (unpublished results). The 100 ns simulation required four months of CPU time on an SGI Onyx workstation. The coordinates were sampled every 0.5 ps, leading to a total number of 200 000 snapshots which required 400 Mbyte of disk space.

To separate intramolecular from residual reorientational overall motions, the coordinates were postprocessed by aligning the principal axis system (PAS) of the molecular inertia tensor, which is only weakly modulated by the internal motions, for every frame with a reference frame (snapshot after 10 ns). Since there is no rigorous separation of internal and overall motion, alternative methods of removal of overall motion are also applicable, such as a least-squares superposition of atoms. For the computation of NMR relaxation rate constants, the molecular tumbling was introduced with the assumption that the overall tumbling motion is isotropic.

(35) (a) Schmidt, J. M.; Brüschweiler, R.; Ernst, R. R.; Dunbrack, R. L., Jr.; Joseph, D.; Karplus, M. *J. Am. Chem. Soc.* **1993**, *115*, 8747−8756. (b) Brunne, R. M.; van Gunsteren, W. F.; Brüschweiler, R.; Ernst, R. R. *J. Am. Chem. Soc.* **1993**, *115*, 4764−4768.

(36) Brüschweiler, R.; Roux, B., Blackledge, M., Griesinger C., Karplus, M.; Ernst, R. R. *J. Am. Chem. Soc.* **1992**, *114*, 2289−2302.

3.2. Phenylalanine Motions. In the present simulation, the four phenylalanine side chains show a characteristic behavior in the χ_1, χ_2 rotational dynamics (Figure 2b). F5, F9, and F10 stay for more than 95% of the simulation time in the $\chi_1 = -60°$ (I) rotamer. By contrast, F6 shows frequent interconversion between the −60° and −180° (II) rotamers and rare visits of the $\chi_1 = 60°$ (III) rotamer. The χ_2 dynamics can be characterized for all four phenylalanines by local fluctuations and by 180° jumps. During the 100 ns simulation time the aromatic rings of F5 and F10 show only 9 and 8 transitions, respectively, whereas F6 and F9 display better statistics with 313 and 20 transitions, respectively. Since the behaviors of F5 and F10 strongly resemble that of F9, only F6 and F9 are further analyzed in the following. The time dependence of χ_1 and χ_2 for F6 and F9 is shown in Figure 3.

Equilibrium properties and correlation effects between the χ_1 and χ_2 motions are conveniently visualized by scatter plots (Figure 4). F9 populates two substates (Figure 4c) which correspond to a $\Delta\chi_2 = 180°$ ring flip. Both χ_1 and χ_2 exhibit nearly Gaussian distributions as is visible from the histograms in Figure 4c. The "principal axes" of the distributions are parallel to the χ_1 and χ_2 axes, indicating that the local fluctuations are not correlated. The slightly unequal population of the two energetically equivalent states is due to the limited MD simulation time. F6, populating six different substates, has a more complex behavior. Interestingly, the equilibrium χ_2 values depend on the χ_1 rotameric state. Thus, the χ_1 and χ_2 jump motions are correlated due to interactions of the side chain with other residues. As in F9, the local χ_1, χ_2 distributions of F6 have nearly Gaussian character. A statistical analysis of the local dihedral angle fluctuations and rotamer populations is given in Table 1. The fluctuations in χ_1 refer to the usual definition of χ_1 as the dihedral angle $N-C^\alpha-C^\beta-C^\gamma$. For the order parameter of the $C^\beta-H^\beta$ bond vector, however, the fluctuations of the dihedral angle $N-C^\alpha-C^\beta-H^\beta$ are more relevant. They are given in parentheses in Table 1 as well. Because the potential for the C−C−H bond angle is softer than for the

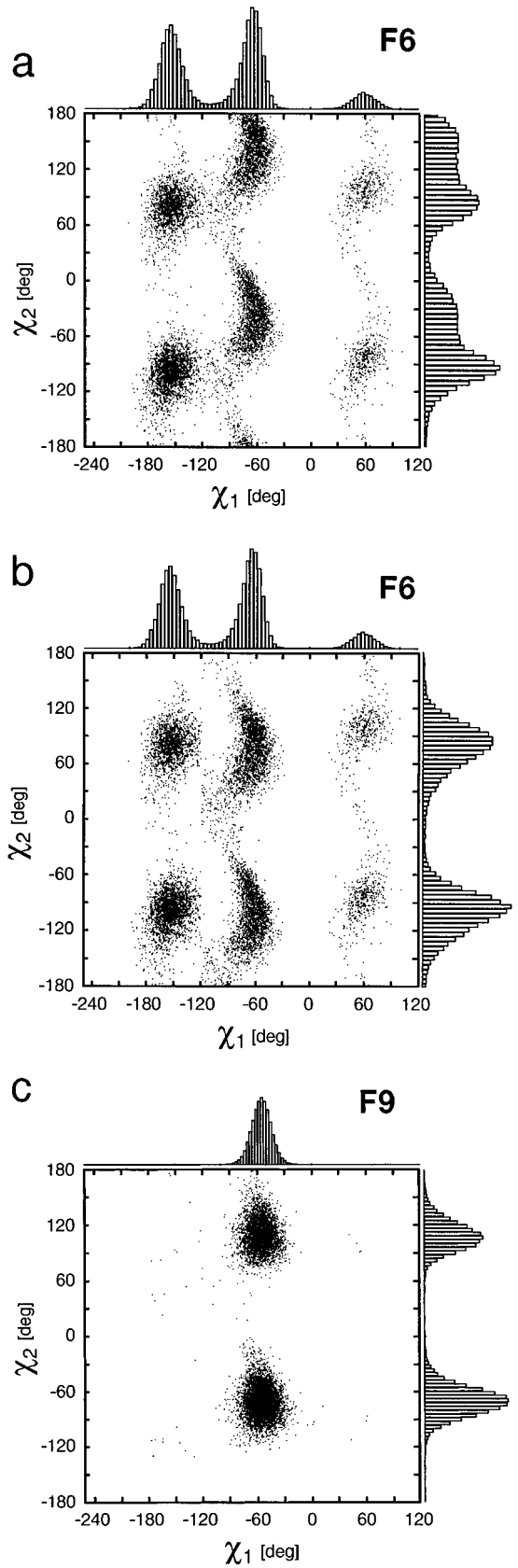

Figure 4. Scatter plots of χ_2 vs χ_1 over the 100 ns trajectory for (a) F6 and (c) F9. A total of 10 000 snapshots are shown, and the individual distributions of χ_1 and χ_2 are plotted as histograms along the corresponding axes. (b) χ_1, χ_2 distribution of F6 after elimination of the correlation between χ_1 and χ_2 jumps (see text).

C−C−C bond angle, the dihedral angle N−C$^{\alpha}$−C$^{\beta}$−H$^{\beta}$ shows slightly larger fluctuations than N−C$^{\alpha}$−C$^{\beta}$−C$^{\gamma}$.

Local dihedral angle motion can be more quantitatively assessed by the computation of the potentials of mean force $W_i(\chi_i) = -kT \ln \rho_i(\chi_i)$,[30] where $\rho_i(\chi_i)$ are the probability density functions of the χ_1 or the χ_2 dihedral angle. The resulting potentials of mean force for F6 and F9 are shown in Figure 5. Superimposed are parabolic approximations for the potential, which agree well with the original potentials for free energies lower than about 6 kJ/mol above the minimum. Thus, at room temperature, F6 and F9 experience for more than 90% of the time a nearly perfect harmonic potential. These findings are supported by the correlation function analysis presented in the following section.

3.3. NMR Correlation Functions and Plateau Values. Carbon-13 nuclear spin relaxation of the phenylalanine side chains is governed by dipolar and chemical shielding anisotropy (CSA) interactions. The power spectral density functions determining the relaxation parameters can be calculated as the Fourier transforms of the dipolar and CSA correlation functions. In most cases, it can be safely assumed that the overall molecular tumbling and the intramolecular conformational mobilities are uncorrelated. The angular part of the cross-correlation function of two axially-symmetric tensor interactions, μ and ν, or of the autocorrelation function of an interaction, $\mu = \nu$, is then, assuming isotropic rotational diffusion with correlation time τ_c, given by

$$C^{\mathrm{tot}}_{\mu\nu}(t) = \mathrm{e}^{-|t|/\tau_c} C^{\mathrm{int}}_{\mu\nu}(t) \tag{1}$$

where the internal part $C^{\mathrm{int}}_{\mu\nu}(t)$ is calculated from the MD trajectory, sampled at N snapshots with time increment Δt, by the expression

$$C^{\mathrm{int}}_{\mu\nu}(k\Delta t) = \frac{1}{(N-k)} \sum_{i=1}^{N-k} \frac{3(\mathbf{e}_{\mu,i+k} \cdot \mathbf{e}_{\nu,i})^2 - 1}{2} \tag{2}$$

$$(k = 0, ..., N-1)$$

where $\mathbf{e}_{\mu,i}$ is the direction of the symmetry axis of the axially-symmetric interaction tensor μ at snapshot i as seen from a molecular fixed frame. The interaction strengths enter in the form of constant prefactors as given in the Appendix (eqs A26−A30). Equation 2 can also be used for a non-axially-symmetric CSA tensor, utilizing the well-known fact that a non-axially-symmetric tensor can be represented as the sum of two orthogonal axially-symmetric tensors (see the Appendix). We focus here on ^{13}C relaxation of −CH$_n$− fragments where the correlation between relatively slow angular and very fast distance fluctuations can be neglected. Rapid distance fluctuations will only influence the effective average internuclear distances (eq A26).

For $\mu = \nu$, the autocorrelation plateau value of $C^{\mathrm{int}}_{\mu\mu}(t)$ for $t \rightarrow \infty$ corresponds in theory to the order parameter S^2.[12] Since for longer times $k\Delta t$ the statistical uncertainty for $C^{\mathrm{int}}_{\mu\mu}(k\Delta t)$ in eq 2 increases, in practice S^2 is often computed as the average of $(3(\mathbf{e}_{\mu,i} \cdot \mathbf{e}_{\mu,j})^2 - 1)/2$ over all pairs i, j requiring $N(N-1)/2$ evaluations of the scalar product.[37] The same value for S^2 can be obtained more efficiently by the relationship[25]

$$S^2 = 1 - \frac{4\pi}{5} \sum_{m=-2}^{2} \sigma^2_{Y_{2m}} \tag{3}$$

where $Y_{2m}(\theta(t), \varphi(t))$ are second order spherical harmonics and $\sigma_{Y_{2m}}{}^2 = \langle Y_{2m}{}^* Y_{2m} \rangle - \langle Y_{2m}{}^* \rangle \langle Y_{2m} \rangle$ is the second moment of Y_{2m}.

Table 1. χ_1 Rotamer Populations and Local Fluctuation Amplitudes in Antamanide[a]

	$\chi_1 = -60°$		$\chi_1 = 180°$		$\chi_1 = +60°$		χ_2
	p_{I} (%)	$\sigma_{1,\mathrm{I}}$ (deg)	p_{II} (%)	$\sigma_{1,\mathrm{II}}$ (deg)	p_{III} (%)	$\sigma_{1,\mathrm{III}}$ (deg)	σ_2 (deg)
F6	48	12.6 (13.2)[b]	43	13.5 (14.5)[b]	9	13.0 (13.1)[b]	25.7 (32/19/24)[c]
F9	100	12.7 (14.0)[b]	0		0		17

[a] Local fluctuation amplitudes are defined as standard deviations in χ_1 (dihedral angle N $-C^{\alpha}-C^{\beta}-C^{\gamma}$) and χ_2 (dihedral angle $C^{\alpha}-C^{\beta}-C^{\gamma}-C^{\delta 1}$) calculated from the 100 ns SD trajectory. [b] Values in parentheses refer to the dihedral angle $N-C^{\alpha}-C^{\beta}-H^{\beta}$. [c] Fluctuation amplitudes have been evaluated individually for each of the three χ_1 rotamers.

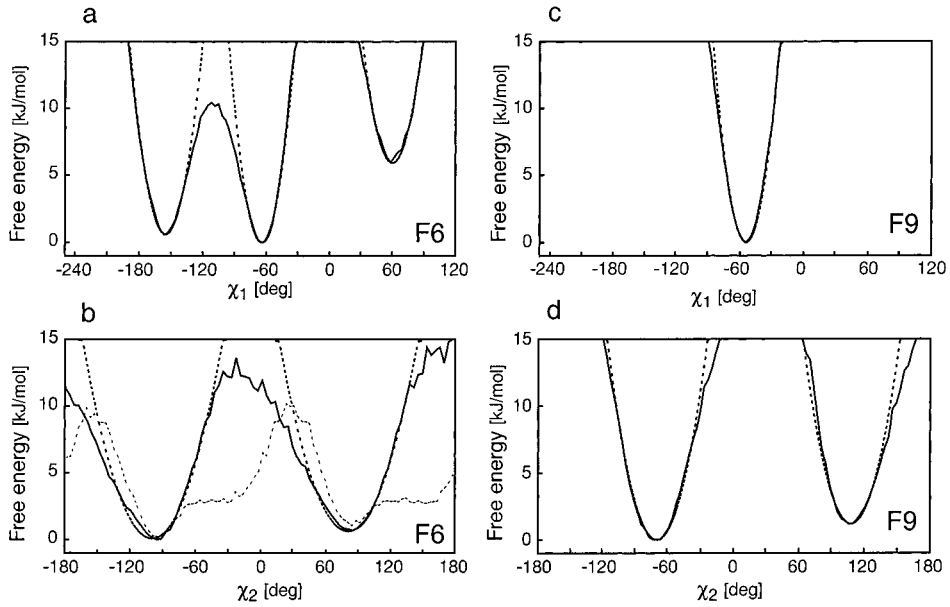

Figure 5. Potentials of mean force along the dihedral angles χ_1 and χ_2 of F6 and F9 extracted from the 100 ns trajectory (solid lines). The dotted lines indicate the best parabolic fits. In (b) the thin dotted line indicates the potential of mean force before elimination of the correlation between χ_1 and χ_2 jumps (see the text).

Equation 3 can be formulated in real quantities by expressing the spherical harmonics in terms of Cartesian coordinates:

$$S^2 = 1 - (3/4)[3\sigma_{z^2}^2 + \sigma_{x^2-y^2}^2 + 4(\sigma_{xy}^2 + \sigma_{yz}^2 + \sigma_{zx}^2)] \qquad (4)$$

where $x(t)$, $y(t)$, and $z(t)$ are the Cartesian components of the internuclear unit vector $\mathbf{e}_i$ at different snapshots i and $\sigma_f^2 = \langle f^2 \rangle - \langle f \rangle^2$ is the variance of the real function $f(\mathbf{e}_i)$. Equation 4 is well suited for the calculation of S^2 for a large number of snapshots avoiding complex arithmetic and requiring only a single loop over the trajectory. It has been used for all S^2 order parameters calculated in this work. Clearly, S^2 is only meaningful if for long times $C_{\mu\mu}^{\mathrm{int}}(t)$ fluctuates with small amplitude about a plateau value. This should be tested by inspection of the correlation function, which can be calculated for long trajectories at a resolution lower than Δt to save computer time.

The correlation functions for F6 and F9 are given in Figure 6. All autocorrelation and cross-correlation functions show a fast initial decay within a few picoseconds. It is of similar magnitude for the corresponding correlation functions of F6 and F9. While for the $C^{\alpha}-H^{\alpha}$ autocorrelation functions the decay is about 10%, it is more pronounced for the $C^{\beta}-H^{\beta}$ vectors, where it is about 15%. In both F6 and F9, the $C^{\zeta}-H^{\zeta}$ vector of the aromatic ring experiences motion very similar to that of $C^{\beta}-H^{\beta}$ vectors since the $C^{\zeta}-H^{\zeta}$ vector is collinear with the $C^{\beta}-C^{\gamma}$ axis and is thus unaffected by motion about χ_2. The amplitude of the fast decay of the autocorrelation and cross-correlation functions of the vectors experiencing motions about χ_1 and χ_2 is even larger (25−40%), reflecting the cumulative effect of the local fluctuations about the two dihedral angles.

For the correlation functions of F6 (except $C^{\alpha}-H^{\alpha}$), the very rapid decay is first followed by a decay with a time constant of about 100 ps, and then by a further decay with a time constant in the 1 ns range. The decay processes are due to the rotameric exchange in χ_1, which is the cause of the small plateau values for all side-chain correlation functions of F6. Note that, for F6 and F9, the vector pairs $C^{\delta 1}-H^{\delta 1}$, $C^{\epsilon 2}-H^{\epsilon 2}$ and $C^{\delta 2}-H^{\delta 2}$, $C^{\epsilon 1}-H^{\epsilon 1}$ behave identically, since they are collinear. In addition, the presence of 180° jumps in χ_2 makes the two pairs equivalent,[16] and all four vectors exhibit identical correlation functions referred to as $C^{\delta\epsilon}-H^{\delta\epsilon}$. The only large-amplitude slow-time-scale mode of F9 is visible in the $C^{\delta\epsilon}-H^{\delta\epsilon}$ correlation function and is due to 180° flips in χ_2 with a time constant of 1.4 ns.

Some further, more detailed observations in Figure 6 are worth mentioning. The two $C^{\beta}-H^{\beta}$ vectors of F6 exhibit nearly indistinguishable correlation functions whereas for F9 a small difference on a nanosecond time scale is visible. The same mode seems to affect the $C^{\alpha}-H^{\alpha}$ and the $C^{\zeta}-H^{\zeta}$ systems as well. It reflects angular motion which does not modulate the χ_1 dihedral angle. The total magnitude of such modes can be visualized by plotting the probability distribution of the tip of the $C^{\beta}-H^{\beta 2}$ vector in the molecule-fixed frame (Figure 7). The nearly Gaussian shaped probability density of this vector on the rotational cone about the $C^{\alpha}-C^{\beta}$ axis demonstrates that the $C^{\beta}-H^{\beta 2}$ vector is in fact dominated by motion about χ_1. However, despite its small amplitude, the influence of the nanosecond mode on spin relaxation can become important as will be discussed in the following section.

To learn more about the sensitivity of the NMR relaxation parameters on the correlated χ_1 and χ_2 motion of F6 (see Figure 4a), NMR correlation functions (eq 2) were calculated for a

(37) Chandrasekhar, I.; Clore, G. M.; Szabo, A.; Gronenborn, A. M.; Brooks, B. R. *J. Mol. Biol.* **1992**, *226*, 239−250.

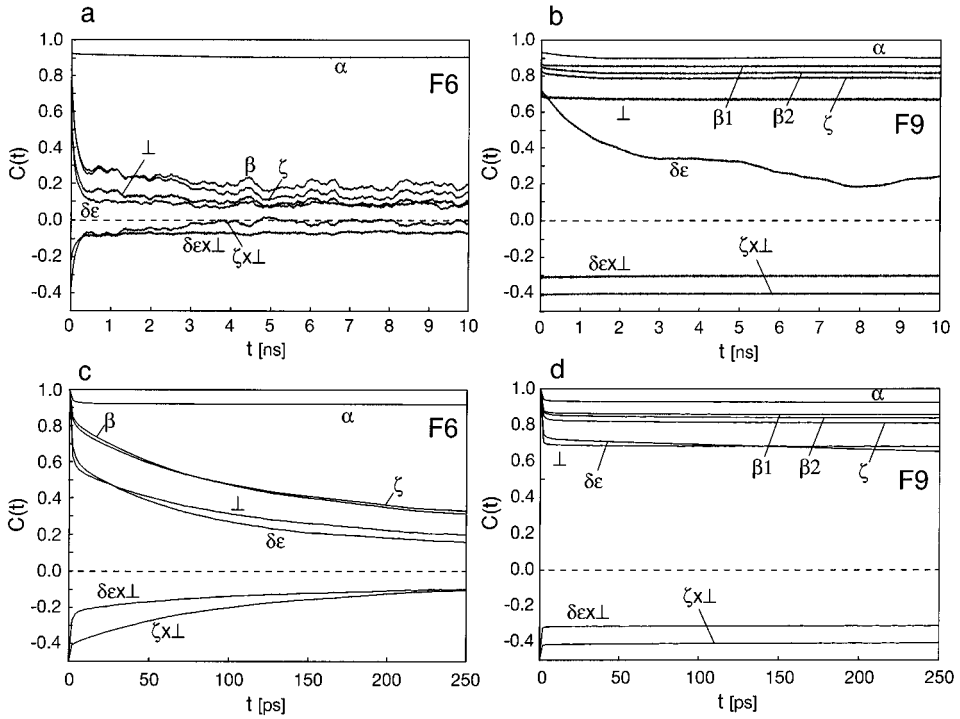

Figure 6. Autocorrelation and cross-correlation functions of F6 and F9 that are relevant for NMR relaxation calculated from the 100 ns trajectory. The time behavior is shown of the autocorrelation funtions of the vectors along $C^{\alpha}-H^{\alpha}$ (α), $C^{\beta}-H^{\beta}$ (β) (average of $C^{\beta}-H^{\beta 1}$ and $C^{\beta}-H^{\beta 2}$ functions), $C^{\delta\epsilon}-H^{\delta\epsilon}$ ($\delta\epsilon$) (average of $C^{\delta}-H^{\delta}$ and $C^{\epsilon}-H^{\epsilon}$ functions), and $C^{\zeta}-H^{\zeta}$ (ζ) and along the direction normal to the ring plane ($\perp$) of F6 and F9. Also given are the cross-correlation functions between the direction of $C^{\delta\epsilon}-H^{\delta\epsilon}$ and the ring normal ($\delta\epsilon \times \perp$) and between the direction of $C^{\zeta}-H^{\zeta}$ and the ring normal ($\zeta \times \perp$). For F9, the correlation functions for $C^{\beta}-H^{\beta 1}$ ($\beta 1$) and $C^{\beta}-H^{\beta 2}$ ($\beta 2$) are slightly different and are plotted separately. Fast-time-scale behavior up to 250 ps is shown in Figure 6c,d for F6 and F9, respectively. While the auto-correlation functions start for $t = 0$ at 1.0, the cross-correlation functions of orthogonal vectors start at $P_2(\cos 90°) = -0.5$.

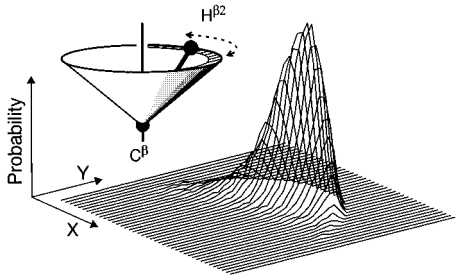

Figure 7. Probability distribution of the tip of the $C^{\beta}-H^{\beta 2}$ vector of F9. The *z* axis is chosen parallel to the average $C^{\alpha}-C^{\beta}$ direction, and the *y* axis points along the average $C^{\beta}-H^{\beta 2}$ bond vector.

second trajectory which was derived from the first one. In the second trajectory, the correlation has been artificially removed by shifting the χ_2 angles of all snapshots populating the $\chi_1 = -60°$ rotamer by $\Delta\chi_2 = -65°$. This largely removes the dependence of the χ_2 equilibrium values on the χ_1 rotameric state (see the scatter plot Figure 4b), and the spatial part of the jump correlation between χ_1 and χ_2 is eliminated. The correlation functions for the original and modified trajectories are given in Figure 8. While the $C^{\delta\epsilon}-H^{\delta\epsilon}$ autocorrelation function, responsible for dipolar relaxation, remains almost unaffected, the ring-normal and cross-correlated CSA correlation functions are quite susceptible to this correlation effect. The latter correlation functions enter only into the relaxation expressions for non-axially-symmetric CSA tensors, as is described in the Appendix in eq A30. Because even at the highest magnetic fields used in this work, the dipolar relaxation exceeds the CSA relaxation by at least a factor of 5, the correlation effects on the measurable relaxation rates remain small. It is estimated using the correlation functions given in Figure 8 that the correlation modifies the relaxation of side-chain ^{13}C by less than 1% and is very difficult to measure. It should be noted, however, that for other side-chain geometries and time scales such correlation effects can become more important.

3.4. Emerging Motional Picture: GAF & Jump Model. From the analysis of the LD trajectory the following motional picture emerges: F6 and F9 undergo Gaussian axial fluctuations about χ_2 combined with 180° flips. For F9, motion about χ_1 is unimodal and Gaussian, whereas for F6, the three rotamers are populated with the ratio 0.48:0.43:0.09. The motion in each rotamer is in good approximation harmonic with correlation times in the picosecond range. We term this motional behavior consisting of local Gaussian axial fluctuations and interrotameric jump motions the "GAF & jump model".

The Gaussian fluctuations in χ_1 and χ_2 can be characterized by fluctuation amplitudes σ_1 and σ_2 and correlation times τ_1 and τ_2, respectively, and the interconversion rate constant between the two rotamers in χ_2 is $k_2 = (\tau_2^{\text{jump}})^{-1}$. For F6, the rotameric exchange in χ_1 is determined by interconversion rate constants $k_{ji} = \tau_{i\rightarrow j}^{-1}$ (i, j = I, II, III), and the corresponding rotamer populations p_i obey the principle of detailed balance $p_i/p_j = k_{ij}/k_{ji}$. An analytical form of the NMR correlation function for the GAF & jump model is described in detail in the Appendix, with the general expression of the relevant NMR correlation function $C_{\mu\nu}(t)$ given in eq A23.

4. Sensitivity Analysis and Consistency Test

The GAF & jump model has been designed to describe the χ_1 and χ_2 fluctuation properties of F6 and F9 observed in the LD simulation. In this section, we test how accurately we can retrieve the relevant parameter values from NMR ^{13}C T_1 and $\{^1H\}^{13}C$ NOE relaxation data calculated directly from the MD correlation functions. Such a test is important, since relaxation parameters depend in a highly nonlinear way on the molecular fluctuation properties. Particular attention is paid to the

Table 2. Fit of 2D GAF & Jump Model Parameters of F9 for Different τ_c Values[a]

	model parameters	fits				direct LD estimate
		$\tau_c = 0.150$ ns	$\tau_c = 0.800$ ns	$\tau_c = 5$ ns	$\tau_c = 15$ ns	
χ_1	σ_1 (deg)	16 ± 0.7 (15)	16 ± 1.2 (15)	13 ± 0.6 (15)	4.5 ± 0.1 (15)	14[b,c]
	$\tau_1^{GAF} = 1/D_1$ (ns)	0.13 ± 0.09 (0.021)	0.122 ± 0.07 (0.020)	0.212 ± 0.05 (0.023)	0.34 ± 0.05 (0.026)	0.025[d]
χ_2	σ_2 (deg)[e]	13 ± 2.0 (13.5)	15 ± 2.0 (13.6)	18 ± 1.7 (12.1)	25 ± 1.5 (10.2)	17[c]
	τ_2^{jump} (ns)	2.6 ± 1.5 (2.6)	2.7 ± 1.5 (2.6)	2.8 ± 0.9 (2.7)	3.1 ± 0.6 (2.7)	2.5

[a] Fitted values after the removal of the 500 ps slow-time-scale contribution to the correlation function (see text) are given in parentheses. The errors limits are determined by a Monte Carlo procedure consisting of 100 fits with random errors of 2% standard deviation added to all T_1 and NOE relaxation data computed from the LD trajectory. [b] Refers to the dihedral angle $N-C^{\alpha}-C^{\beta}-H^{\beta}$. [c] Root-mean-square (rms) dihedral angle fluctuation. [d] Obtained by conversion of the correlation time of the dihedral fluctuation $\tau \approx 1.5$ ps to the value entering the GAF & jump model: $\tau_1^{GAF} = \tau/\sigma_1^2 = 1/D_1$ (see eq A12). [e] $\tau_2^{GAF} < 0.01$ ns for all τ_c values. Estimated value from LD: $\tau_2^{GAF} = 0.02$ ns.

influence of the overall tumbling correlation time τ_c on the extraction of intramolecular motional properties. For this purpose, T_1 and η values have been calculated directly from the trajectory (using eqs 1, 2, A5, A26, A27, and A30) for three distinct phenylalanine side-chain CH systems ($C^{\beta}-H^{\beta}$, $C^{\delta\epsilon}-H^{\delta\epsilon}$, and $C^{\zeta}-H^{\zeta}$) at three different B_0-field strengths corresponding to 400, 600, and 800 MHz proton frequency. This results in $2 \times 3 \times 3 = 18$ relaxation parameters for each side chain. Transverse T_2 relaxation data are not included since in practice they often contain contributions from chemical shift modulations due to slow conformational dynamics. The latter tend to be difficult to separate from the dipolar and CSA relaxation mechanisms considered here, requiring rotating frame $T_{1\rho}$ measurements where often the accessible range of radio-frequency fields is limited.

To obtain accurate analytical expressions, all internal autocorrelation and cross-correlation functions were fitted by a multiexponential decay consisting of six exponentials and a plateau value S^2:

$$C(t) = S^2 + \sum_{i=1}^{6} A_i e^{-t/\tau_i} \quad \text{where} \quad S^2 + \sum_{i=1}^{6} A_i = 1, \quad A_i, \tau_i > 0 \tag{5}$$

While *no* general physical meaning is attributed to the parameters $\{A_i\}$ and $\{\tau_i\}$, this parametrization will allow manipulation of the correlation functions by setting a specific A_i value to zero to study the influence of a specific time-scale range on relaxation. The NMR relaxation parameters were then calculated by inserting eq 5 into eq 1, assuming an overall tumbling correlation time τ_c, followed by analytical Fourier transformation. The equations used for the calculation of T_1 and η are given in the Appendix (eqs A26, A27, and A30). The calculated relaxation parameters include contributions from $^{13}C-^{1}H$ dipolar and ^{13}C CSA relaxation mechanisms. For the phenyl ring, the same CSA tensors have been used as in ref 24 with principal axis values $\sigma_{zz} = 118$ ppm (parallel to the C−H bond), $\sigma_{xx} = -97$ ppm (orthogonal to the ring plane), and $\sigma_{yy} = -21$ ppm (orthogonal to the other two axes). A table containing the $\{A_i\}$ and $\{\tau_i\}$ parameters is included in the Supporting Information.

The tumbling correlation time τ_c has been set to different values to mimic biomolecules of different sizes: 150 ps (corresponding to the tumbling correlation time of antamanide in $CDCl_3$ at 320 K[24]), 800 ps, 5 ns, and 15 ns. For each τ_c value, the GAF & jump model parameters have been determined by a least-squares fit using the simplex algorithm[38] as implemented in the software package MATLAB for matrix manipulations.[39]

For F9, the model consists of Gaussian fluctuations in χ_1 and 180° χ_2 jumps of the ring, between $\chi_2 \cong \pm 90°$. The results of these fits are compiled in Table 2. The indicated error intervals are obtained from a Monte Carlo error analysis, where in 100 separate runs random Gaussian errors with a 2% standard deviation have been added to the T_1 and NOE relaxation data. For the fitting of F6, additional rotameric exchange processes in χ_1 have been included (Table 3). While the general treatment of exchange among the three χ_1 rotamers requires five parameters, the model used for the description of the motion of F6 assumes that two of the three rotamer populations are the same ($p_I = p_{II}$). The transition rate constants involving the third state, $k_{III \to I}$ and $k_{III \to II}$, are not well defined in the simulation due to poor statistics. In the model they are assumed to be identical, $k_{III \to I} = k_{III \to II}$.[40]

For F9 the χ_1 fluctuation amplitude, σ_1, is well reproduced for tumbling correlation times smaller than 5 ns (Table 2). The dependence of σ_1 on τ_c is due to the presence of motion causing reorientation of the $C^{\alpha}-C^{\beta}$ vector, in particular the small amplitude motional mode with $\tau_5 \approx 500$ ps visible in Figure 6b. In fact, removal of this mode from the correlation functions

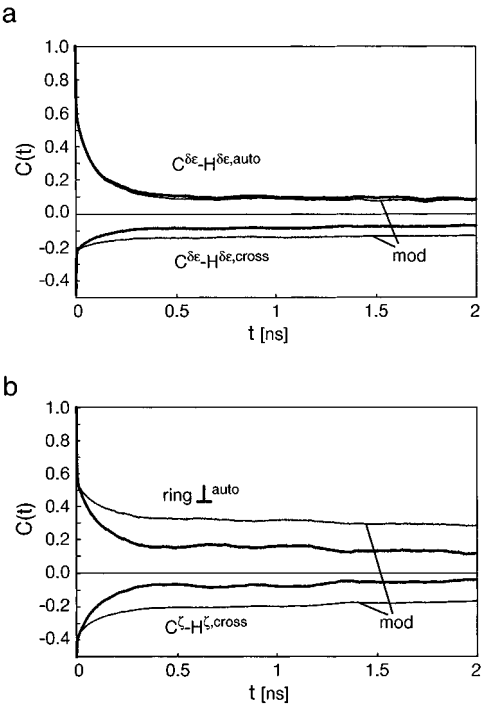

Figure 8. Comparison of the correlation functions with and without elimination of the correlation between jumps between the different minima of F6. The correlation functions of the original and the modified trajectory are given as bold and thin lines, respectively. (a) Autocorrelation function of the $C^{\delta\epsilon}-H^{\delta\epsilon}$ vectors (see the text) and cross-correlation function of the ring normal with the $C^{\delta\epsilon}-H^{\delta\epsilon}$ vectors. (b) Autocorrelation function of the ring normal and cross-correlation function of the ring normal with the $C^{\zeta}-H^{\zeta}$ vectors.

(38) Nelder, J. A.; Mead, R. *Comput. J.* **1964**, *7*, 308−313.
(39) *MATLAB Reference Guide*; The Math Works Inc.: Natick, MA, 1992.
(40) Tsutsumi, A. *Mol. Phys.* **1979**, *37*, 111−127.

Table 3. Fit of 2D GAF & Jump Model Parameters of F6 for Different τ_c Values[a]

	model parameters	fits				direct LD estimate
		$\tau_c = 0.150$ ns	$\tau_c = 0.800$ ns	$\tau_c = 5$ ns	$\tau_c = 15$ ns	
χ_1	σ_1 (deg)[b]	15 ± 5.9	15.4 ± 3.4	15.9 ± 3.0	15.8 ± 2.5	13.8[c,d]
	p_{III}[e] (%)	9 ± 5	9 ± 3	10 ± 1	10 ± 1	9
	$p_I = p_{II}$[e] (%)	45.5 ± 2.5	45.5 ± 1.5	45 ± 0.5	45 ± 0.5	$p_I = 43$ $p_{II} = 48$
	$\tau^{jump}_{III\to I} = \tau^{jump}_{III\to II}$ (ns)[e]	3.2 ± 1.8	3.2 ± 1.4	3.2 ± 0.2	3.2 ± 0.2	3.3[f]
	$\tau^{jump}_{I\leftrightarrow II}$ (ns)[e]	0.11 ± 0.07	0.11 ± 0.05	0.15 ± 0.01	0.18 ± 0.01	0.12[f]
χ_2	σ_2 (deg)[g]	18 ± 0.2	17 ± 0.2	16 ± 0.4	13 ± 0.8	25.7
	τ^{jump}_2 (ns)	0.37 ± 0.02	0.50 ± 0.01	0.63 ± 0.01	0.49 ± 0.04	(0.16)[h]

[a] The error limits given are determined by a Monte Carlo procedure consisting of 100 fits with random errors of 2% standard deviation added to all T_1 and NOE relaxation data computed from the LD trajectory. [b] $\tau_1^{GAF} < 0.01$ ns for all τ_c values. Estimated value from LD: $\tau_1^{GAF} = 0.02$ ns. [c] Refers to the dihedral angle $N-C^{\alpha}-C^{\beta}-H^{\beta}$. [d] Root-mean-square (rms) dihedral angle fluctuation. [e] Absolute rotamer identification is not possible from fitting relaxation data. [f] $\tau^{jump}_{i\to j} = p_i/N_{i\to j}$ where $N_{i\to j}$ is the number of transitions from rotameric state i to rotameric state j. [g] $\tau_2^{GAF} < 0.01$ ns for all τ_c values. Estimated value from LD: $\tau_1^{GAF} = 0.02$ ns. [h] See caption of Figure 3.

for $C^{\beta}-H^{\beta}$ and $C^{\zeta}-H^{\zeta}$ yields excellent agreement with σ_1 determined directly from the LD trajectory irrespective of τ_c (values in parentheses in Table 2). Despite its small amplitude, this mode also has an effect on the apparent internal motional correlation time τ_1 about χ_1 as is seen by comparing the fitted τ_1 values in the presence and the absence of this mode (values in parentheses). For slower molecular tumbling, the influence of this mode on the relaxation rates becomes increasingly dominant, and for $\tau_c = 15$ ns the fit of the computed NMR data seriously underestimates σ_1. This unexpected behavior can be understood as follows. Heteronuclear T_1 and η values sample the power spectral density $J(\omega_i)$ at frequencies $\omega_i = \omega_C$, $\omega_C \pm \omega_H$. $J(\omega_i)$, which corresponds to a sum of Lorentzian functions, becomes small for either very large intramolecular correlation times τ ($\omega_i\tau \gg 1$) or very short correlation times ($\omega_i\tau \ll 1$) and is largest in an intermediate range, where $\omega_i\tau \approx 1$. The 500 ps motional mode falls into this intermediate range and dominates for slow tumbling the spectral density contributions originating from the fast Gaussian fluctuations. Hence, the apparent effective intramolecular rate constant τ_1^{-1} and the associated fluctuation amplitude are both reduced. This phenomenon is not specific for the GAF & jump model and occurs also, e.g., in a model-free analysis. To our knowledge, this phenomenon has not been addressed in the literature and should become relevant in the context of relaxation studies of large biomolecules. T_1 and η values remain highly sensitive to internal motions in the $\omega_i\tau \approx 1$ regime even for large tumbling correlation times while very fast and very slow intramolecular processes become relaxation-inactive. In this limit, the system assumes nearly solid-like behavior. If T_2, which samples also $J(0)$, is included in the fit, the very fast internal motions maintain their dominant influence on T_2 irrespective of τ_c.

For σ_2 of F9, the fitted value for σ_2^{fit} is smaller than σ_2^{LD} for short τ_c due to the statistical error for the χ_2 180° jumps during the 100 ns LD simulation, where a population ratio of the two χ_2 rotamers of 0.53:0.47 is observed. Since for symmetry reasons, the GAF & jump model intrinsically assumes equal populations, the model overestimates the amount of jump motion present compared to the LD target. The fit compensates for this by reducing the σ_2 value, and thus underestimates σ_2. For larger τ_c, σ_2 increases steadily to compensate for the reduced σ_1 value, because the relevant ring vectors, such as $C^{\delta\epsilon}-H^{\delta\epsilon}$, which experience motion about χ_2 and therefore determine σ_2, are not significantly affected by the 500 ps mode. Again, removal of this mode yields more consistent fits for σ_2, exhibiting a slight decrease for increasing τ_c. The fitted τ_2^{jump} time constants (Table 2) are rather insensitive to τ_c and are close to the LD estimates.

The consistency analysis of F6, summarized in Table 3, yields a slightly overestimated fitted σ_1. The reason lies in the presence of phenyl ring bending motion, which is independent of dihedral angle fluctuations about χ_1 and χ_2 and which reduces the order parameter S^2 of $C^{\zeta}-H^{\zeta}$ to 0.16 compared to 0.20 for $C^{\beta}-H^{\beta}$. Since this additional motion is not explicitly included in the GAF & jump model, it leads to an increased fitted value of $\sigma_1 \approx 15.5°$ compared to 13° estimated from the LD trajectory. The $C^{\delta\epsilon}-H^{\delta\epsilon}$ vectors, on the other hand, are less affected by the bending mode, and the fitted values of σ_2 are underestimated, compensating for the overestimated motion about χ_1. As for F9, the two phenyl ring rotamers are not exactly 1:1 populated in the LD simulation due to the finite length of the trajectory, causing a decrease of the fitted σ_2 value.

In summary, application of the GAF & jump model to the simulation data gives for both residues reasonably good agreement, as long as the overall tumbling of the molecule is not too slow. For $\tau_c \le 5$ ns the σ_1 and σ_2 fluctuation parameters can be retrieved with reasonable accuracy from the T_1 and NOE data calculated from the LD trajectory at three different B_0 field strengths. The intramolecular diffusion constants are remarkably sensitive to the presence of a small-amplitude slow-time-scale dynamical mode. In particular, for $\tau_c > 5$ ns this mode starts to contribute significantly to the relaxation parameters, biasing strongly the estimates for σ_1 and σ_2 as this additional intermediate-rate motion is not explicitly parametrized in the model.

5. Application to Experimental Data

The GAF & jump model can now be applied to the experimental relaxation data of F6 and F9 of antamanide published previously in ref 24 where 31 relaxation parameters have been measured and evaluated for each of the four phenylalanine residues. The present analysis is restricted to the 25 standard ^{13}C T_1 and $\{^1H\}^{13}C$ NOE parameters measured at three different B_0 fields of 200 (only T_1), 400, and 600 MHz proton frequency at 320 K. (The six parameters related to heteronuclear two-spin order, which are not widely used, were found to have minor influence on the fitting results and were not included here.) The set of optimum parameter values of the GAF & jump model, determined by least squares fits, is given in Table 4.

For F6, a three-site jump model has been applied to the χ_1 motion, based on the results of sections 3 and 4. Two populations and two jump rate constants were assumed to be equal: $p_I = p_{II}$, $\tau^{jump}_{III\to I} = \tau^{jump}_{III\to II}$. Table 4 shows that the local GAF motion leads to an rms angular fluctuation of $10.5 \pm 5°$ and to nearly equal populations of the three rotamers with $p_I = p_{II} = 32 \pm 13\%$ and $p_{III} = 36 \pm 25\%$, whereby the uncertainty

Table 4. Fit of the Model Parameters of F6 and F9 to the Experimental Data[a] ($\tau_c = 150$ ps)

		F6	F9
χ_1	σ_1 (deg)[b]	10.5 ± 5	16.5 ± 3.5
	p_{III}[c] (%)	36 ± 25	
	$p_I = p_{II}$[c] (%)	32 ± 13	
	$\tau^{jump}_{III\rightarrow I} = \tau^{jump}_{III\rightarrow II}$ (ns)	2.3 ± 1.5	
	$\tau^{jump}_{I\leftrightarrow II}$ (ns)	0.76 ± 0.22	
χ_2	σ_2 (deg)[d]	18.4 ± 4.5	13.8 ± 4.5
	τ_2^{jump} (ns)	>4	0.76 ± 0.33

[a] Experimental ^{13}C T_1 at 200, 400, and 600 MHz and $\{^1H\}^{13}C$ NOE values at 400 and 600 MHz at 320 K have been used from ref 24. Errors are calculated using error propagation. [b] $\tau_1^{GAF} < 0.01$ ns. [c] The relaxation data are rather insensitive to the exact population numbers for this tumbling regime ($\tau_c = 150$ ps) (see the text). [d] $\tau_2^{GAF} < 0.01$ ns.

of the numerical values is high due to the relatively large transfer time constants $\tau^{jump}_{III\rightarrow I} = \tau^{jump}_{III\rightarrow II} = 2.3 \pm 1.5$ ns and $\tau^{jump}_{I\leftrightarrow II} = 0.76 \pm 0.22$ ns. The time constant for the local GAF motion is fast and not accurately measurable with $\tau_1^{GAF} < 10$ ps. The GAF of χ_2 has an rms value of $18.4 \pm 4.5°$, again with a very short time constant $\tau_2^{GAF} < 10$ ps, while the two-site jump process is slow, $\tau_2^{jump} > 4$ ns, with little influence on the relaxation behavior.

It is interesting to compare these results with the analysis of the full 31 relaxation parameters given in ref 24 where several simpler models have been considered. The present analysis can be compared with the three-site/two-site jump model A_1B_2 and with the restricted three-site/two-site jump model C_1B_2.[24] No exact agreement with either model is expected because in the present case, one χ_1 transition is faster than the other two, while for the restricted three-site model, two transitions are allowed while the third one is forbidden. For the inverse average rate constant of the χ_1 jumps, $1/\bar{\tau}_1^{jump} = (1/\tau^{jump}_{I\leftrightarrow II} + 1/\tau^{jump}_{I\rightarrow III} + 1/\tau^{jump}_{III\rightarrow I})/3$, one finds the values $\bar{\tau}_1^{jump}$ (GAF + jump) = 1340 ps, $\bar{\tau}_1^{jump}$ (model A_1B_2) = 785 ps, and $\bar{\tau}_1^{jump}$ (model C_1B_2) = 715 ps. Although the error limits of the involved τ values are considerable, one can attribute the slower jump process in the GAF & jump model to the separation of the motion into jump processes and fast Gaussian axial fluctuations.

The previous analysis[24] delivered for the two-site jump motion of F6 about χ_2 a well-defined correlation time $\tau_2^{jump} = 1/k_2 = 81.6 \pm 8$ ps (assuming model C_1B_2). In the present analysis where this motion has been divided into a local GAF motion and a superimposed two-site jump process, the corresponding correlation times are ill-determined with $\tau_2^{GAF} < 10$ ps and $\tau_2^{jump} > 4000$ ps. The latter has no effect on relaxation, and the only relevant motional parameter is $\sigma_2 = 18.4 \pm 4.5°$, reflecting the partial averaging of the involved interactions. The considerably larger value of τ_2^{jump} determined from the experimental data in comparison to the values from the LD simulation (see Table 3) can at least partially be explained by the elevated temperature of 400 K in the simulation.

The relaxation-active motion of F9 can be described by a standard GAF model for χ_1 with $\sigma_1 = 16.5 \pm 3.5°$ and $\tau_1^{GAF} < 10$ ps while for χ_2 GAF & jump motion seems appropriate. The fluctuations with $\sigma_2 = 13.8 \pm 4.5°$ are again fast with $\tau_2^{GAF} < 10$ ps and have a mere averaging effect. On the other hand, the two-site jump motion has with $\tau_2^{jump} = 760 \pm 330$ ps a correlation time that weakly influences relaxation.

The F9 results can be compared with the model E_1B_2 of ref 24 with restricted rotational diffusion and a restriction angle $\phi_{max} = 32 \pm 3°$ in χ_1 and two-site jump motion in χ_2. The rms fluctuation amplitude σ_1^{rect} corresponding to motion in a rectangular potential of half-width ϕ_{max} is given by $\sigma_1^{rect} = \phi_{max}/\sqrt{3} = 18.5 \pm 2°$ and is well comparable with the presently determined value of $\sigma_1^{GAF} = 16.5 \pm 3.5°$. The corresponding correlation time, indicated as $\tau_1 = 200$ ps in ref 24, is ill-determined and has to be considered as an upper limit. This becomes obvious from the error surfaces of Figures 4 and 5 in ref 24. It is not in true contradiction to the presently found value $\tau_1^{GAF} < 10$ ps.

The previous analysis with the E_1B_2 model of ref 24 led to a χ_2 jump correlation time $\tau_2^{jump} = 1/k_2 = 132.2 \pm 12$ ps while here a corresponding correlation time $\tau_2^{jump} = 760 \pm 330$ ps was found. The discrepancy again shows that by taking into account Gaussian axial fluctuations in χ_2 the relaxation data no longer require a significant relaxation contribution from the two-state jump process, leading to a long and ill-determined correlation time τ_2^{jump}.

The derived approximate populations of the three χ_1 rotamers can also be compared with a population analysis based on the measured *J*-coupling constants.[41,45,46] The most reliable values known today stem from J. M. Schmidt:[41] For F6, $p_I = 30\%$, $p_{II} = 22\%$, and $p_{III} = 48\%$; and for F9, $p_I = 88\%$, $p_{II} = 12\%$, and $p_{III} = 0\%$. They are in qualitative agreement with the present findings. It should be noted that a relaxation analysis is often rather insensitive to the accurate population numbers unless the jump rate constant is in its most sensitive range. For this reason, it is advisable to combine relaxation and *J*-coupling measurements for achieving a better accuracy of the motional parameters.

Conclusion

Molecular dynamics simulations are widely used to compute spectroscopic and scattering properties for direct comparison with experimental data.[29] We use here an extended LD trajectory for the construction of potentials of mean force, which cover most of the NMR relaxation-active motions and which are suitable for deriving analytical expressions of the NMR correlation functions. The resulting model contains a minimal number of parameters whose values can be determined by comparison with experimental data. The deduction of qualitative features of the analytical model from the LD simulation represents an improvement over the otherwise often subjective process of model selection in the course of data interpretation.

In this study, the GAF & jump model emerged for the phenylalanine side-chain motion in antamanide and allowed us to attribute motion reflected in NMR relaxation data to the relevant χ_1 and χ_2 motional degrees of freedom. A sensitivity analysis yielded valuable insight into the interplay between correlation times, motional amplitudes, and experimentally accessible relaxation parameters. It also demonstrates the feasibility and limitations of extracting the relevant motional parameters that determine experimental relaxation data.

This protocol is particularly suitable to describe the dynamics of a subsystem involving a relatively small number of motional modes, such as an amino acid side chain attached to a relatively rigid polypeptide backbone. In cases of slow, relaxation-inactive backbone mobility that may influence the side-chain dynamics,

(41) Schmidt, J. M. To appear in *Supramol. Struct. Funct.*
(42) Zare, R. *Angular Momentum*; Wiley-Interscience: New York, 1988.
(43) Brüschweiler, R.; Case, D. A. *Prog. NMR Spectrosc.* **1994**, *26*, 27−58.
(44) Werbelow, L. G. In *NMR Probes of Molecular Dynamics*; Tycko, R., Ed.; Kluwer: Dordrecht, The Netherlands, 1994; pp 223−263.
(45) Griesinger, C.; Sørensen, O. W.; Ernst, R. R. *J. Magn. Reson.* **1987**, *75*, 474−492.
(46) Kessler, H.; Müller, A.; Pook, K.-H. *Liebigs Ann. Chem.* **1989**, 903−912. Kessler, H.; Bats, J. W.; Lautz, J., Müller, A. *Ibid.* **1989**, 913−928.

it is possible to investigate the side-chain dynamics and the resulting NMR relaxation independently for several backbone conformations and to average the results. In many situations, one can expect that the qualitative features of the side-chain dynamics are not affected by the backbone mobility such that the study of a single backbone conformation provides sufficient information for establishing a motional model for the side chain(s) under investigation.

Situations are conceivable where the proposed approach becomes less suitable. For highly flexible molecules with numerous degrees of freedom requiring a large number of model parameters, it may be difficult to obtain sufficiently good statistics to derive a reliable motional model. Moreover, the emerging model may be too complicated to allow for analytical expressions of the NMR correlation functions. In biomolecules with a rather well-defined average structure, on the other hand, we can envisage a large class of motional processes where the described protocol is promising for deducing motional properties that are of relevance for understanding the molecule's function.

The approach presented here combines complementary information from molecular dynamics simulation and NMR relaxation. Its application to side-chain motion illustrates the necessity for such a unified approach to overcome the inherent ambiguity of the relaxation data with respect to their detailed physical interpretation.

Acknowledgment. Dr. Thomas Schulte-Herbrüggen is gratefully acknowledged for stimulating discussions. This research was supported by the Swiss National Science Foundation.

Supporting Information Available: A table giving the amplitudes A_i and time scales τ_i of eq 5 which characterize the correlation functions of F6 and F9 derived from the MD simulation (1 page). See any current masthead page for ordering and Internet access instructions.

Appendix

Motion in the 2D Harmonic Potential. We consider a molecular side chain with two rotational degrees of freedom given by the dihedral angles $\boldsymbol{\chi} = (\chi_1, \chi_2)$ and the 2D harmonic potential

$$V(\chi_1, \chi_2) = A\chi_1^2 + 2C\chi_1\chi_2 + B\chi_2^2 \tag{A1}$$

We select, for the moment, the origin of χ_1 and χ_2 such that $\langle\chi_1\rangle = 0$ and $\langle\chi_2\rangle = 0$. Using a standard procedure, the probability distribution is obtained by transforming to normal coordinates χ_1' and χ_2':

$$V(\chi_1', \chi_2') = \lambda_1\chi_1^{2'} + \lambda_2\chi_2^{2'} \tag{A2}$$

where $\lambda_{1,2} = (A + B \pm ((A - B)^2 + 4C^2)^{1/2})/2$, $\boldsymbol{\chi}' = \mathbf{R}\boldsymbol{\chi}$,

$$\mathbf{R} = \begin{bmatrix} \cos\alpha & \sin\alpha \\ -\sin\alpha & \cos\alpha \end{bmatrix}$$

and $\alpha = \text{atan}((\lambda_1 - A)/C)$ where $(\cos\alpha, \sin\alpha)^T$ is the eigenvector to λ_1. α is the tilt angle of the principal axis of the ellipse defined by eq A1 with respect to the χ_1 axis. χ_1' and χ_2' are stochastically independent random variables with Gaussian probability distributions

$$p(\chi_i')\,\mathrm{d}\chi_i' = (2\pi\sigma_i^2)^{-1/2}\exp(-\chi_i'^2/2\sigma_i^2)\,\mathrm{d}\chi_i' \quad (i = 1, 2) \tag{A3}$$

with variances $\sigma_i^2 \propto k_B T/\lambda_i$, where T is the absolute temperature. χ_1 and χ_2 are also Gaussian distributed with $\sigma_{\chi_1}^2 = \langle\chi_1^2\rangle - \langle\chi_1\rangle^2 = (\cos^2\alpha)\sigma_1^2 + (\sin^2\alpha)\sigma_2^2$ and $\sigma_{\chi_2}^2 = (\sin^2\alpha)\sigma_1^2 + (\cos^2\alpha)\sigma_2^2$. The correlation coefficient r between χ_1 and χ_2 is determined by

$$r = \frac{\langle\chi_1\chi_2\rangle}{\sigma_{\chi_1}\sigma_{\chi_2}} = (\cos\alpha\,\sin\alpha)\frac{(\sigma_1^2 - \sigma_2^2)}{\sigma_{\chi_1}\sigma_{\chi_2}} \tag{A4}$$

Thus, $r = 0$ for $\sigma_1 = \sigma_2$ or $\alpha = 0, \pi/2$, and $r = \pm 1$ for $\sigma_1 = 0$ or $\sigma_2 = 0$ (if $\alpha \neq 0, \pi/2$). Although the relevant NMR correlation functions calculated from the LD trajectory do not show significant correlations between the local fluctuations of χ_1 and χ_2 ($|r| \ll 1$), the following treatment includes this possibility.

NMR Correlation Functions. The NMR correlation functions are calculated here for an axially-symmetric second-rank tensor, such as an internuclear vector $\mathbf{e}_i$, pointing in a coordinate system which is rigidly attached to the phenylalanine ring (ring system) along the (time-independent) direction $\Omega_i^{\text{ring}} = (\theta_i, \varphi_i)$. The ring system has its z axis parallel to the internuclear $C^\gamma - C^\zeta$ vector and the x axis lies in the ring plane, while the y axis is perpendicular to the plane. The ring system is attached to the polypeptide backbone via the two dihedral angles $\chi_1(t)$ and $\chi_2(t)$, whose axes intersect at the $C^\alpha - C^\beta - C^\gamma$ bond angle $\beta = 109°$. The backbone frame is related to the laboratory frame by a rotation through the three time-dependent Euler angles, specified by $\Phi(t)$.

In isotropic liquids, the angular part of the power spectral density function of two normalized axially-symmetric rank 2 tensors μ and ν is

$$J_{\mu\nu}(\omega) = \int_{-\infty}^{\infty} C_{\mu\nu}(t)\mathrm{e}^{-i\omega t}\,\mathrm{d}t \tag{A5}$$

with the correlation function $C_{\mu\nu}(t)$ given by

$$C_{\mu\nu}(t) = 4\pi\langle Y_{20}(\Omega_\mu^{\text{lab}}(t))\; Y_{20}{}^*(\Omega_\nu^{\text{lab}}(0))\rangle \tag{A6}$$

where $\Omega_i^{\text{lab}}(t)$ describes the orientation of $\mathbf{e}_i$ in the laboratory frame. Starting out from $Y_{2k}(\Omega_\mu^{\text{ring}})$, $Y_{20}(\Omega_\mu^{\text{lab}}(t))$ is obtained by four successive rotations: (i) rotation about $-\chi_2$, (ii) rotation about the y axis of the ring system by the bond angle $\pi - \beta$, (iii) rotation about $-\chi_1$, and (iv) overall rotational tumbling $\Phi(t)$. Using the transformation properties of spherical harmonics,[42] one obtains

$$Y_{20}(\Omega_\mu^{\text{lab}}(t)) = \sum_{k,l=-2}^{2} D_{l0}^{(2)}(\Phi(t))\, D_{kl}^{(2)}(-\chi_2(t), \pi-\beta, -\chi_1(t))\, Y_{2k}(\Omega_\mu^{\text{ring}}) \tag{A7}$$

where $D_{kl}^{(2)}(\alpha,\beta,\gamma)$ denote Wigner matrix elements:

$$D_{kl}^{(2)}(\alpha,\beta,\gamma) = \mathrm{e}^{-ik\alpha}\, \mathrm{d}_{kl}^{(2)}(\beta)\, \mathrm{e}^{-il\gamma} \tag{A8}$$

Insertion of eqs A7 and A8 into eq A6 yields

$$C_{\mu\nu}(t) = 4\pi \sum_{k,l,k',l'=-2}^{2} \langle D_{l0}^{(2)}(\Phi(t))\, D_{l'0}^{(2)}{}^*(\Phi(0))\rangle \times \langle \mathrm{e}^{ik\chi_2(t)+il\chi_1(t)}\mathrm{e}^{-ik'\chi_2(0)-il'\chi_1(0)}\rangle\, \mathrm{d}_{kl}^{(2)}(\pi-\beta)\, \mathrm{d}_{k'l'}^{(2)}(\pi-\beta) \times Y_{2k}(\Omega_\mu^{\text{ring}})\, Y_{2k'}{}^*(\Omega_\nu^{\text{ring}}) \tag{A9}$$

The angular brackets indicate a time average, whereby independence between internal and overall tumbling motion has been assumed. For isotropic tumbling, one obtains

$$\langle D^{(2)}_{l0}(\Phi(t))\, D^{(2)}_{l'0}{}^*(\Phi(0))\rangle = \langle D^{(2)}_{l0}(\Phi(t))\, D^{(2)}_{-l'0}{}^*(\Phi(0))\rangle = (1/5)\mathrm{e}^{-6Dt}\delta_{ll'} \quad \text{(A10)}$$

Transformation to normal coordinates according to eq A2 with the abbreviations $c = \cos\alpha$ and $s = \sin\alpha$ yields

$$C_{\mu\nu}(t) = \sum_{k,k',l=-2}^{2} \langle \mathrm{e}^{ik(s\chi_1'(t)+c\chi_2'(t))+il(c\chi_1'(t)-s\chi_2'(t))} \times \mathrm{e}^{-ik'(s\chi_1'(0)+c\chi_2'(0))-il(c\chi_1'(0)-s\chi_2'(0))}\rangle \times (4\pi/5)\mathrm{e}^{-6Dt}\, \mathrm{d}^{(2)}_{kl}(\pi-\beta)\, \mathrm{d}^{(2)}_{k'l}(\pi-\beta)\, Y_{2k}(\Omega^{\mathrm{ring}}_{\mu})\, Y_{2k'}{}^*(\Omega^{\mathrm{ring}}_{\nu}) \quad \text{(A11)}$$

We now take advantage of the fact that harmonic averaging over χ_1' and χ_2' can be carried out independently. The result for averaging in the strong friction limit has been given by Szabo:[28]

$$\langle \mathrm{e}^{im\chi_\alpha'(t)-in\chi_\alpha'(0)}\rangle = \exp\{-(1/2)\sigma_\alpha{}^2[m^2+n^2-2mn\exp\{-D_\alpha t/\sigma_\alpha{}^2\}]\} \quad (\alpha = 1, 2) \quad \text{(A12)}$$

and one obtains

$$C_{\mu\nu}(t) = \frac{4\pi}{5}\mathrm{e}^{-6Dt}\sum_{k,k',l=-2}^{2} \mathrm{d}^{(2)}_{kl}(\pi-\beta)\, \mathrm{d}^{(2)}_{k'l}(\pi-\beta)\, Y_{2k}(\Omega^{\mathrm{ring}}_{\mu}) \times Y_{2k'}{}^*(\Omega^{\mathrm{ring}}_{\nu}) \exp\left\{-\frac{1}{2}\sigma_1{}^2[(1c+ks)^2+(lc+k's)^2 - 2(lc+ks)(lc+k's)\exp\{-D_1 t/\sigma_1{}^2\}]\right\} \times \exp\left\{-\frac{1}{2}\sigma_2{}^2[(kc-ls)^2+(k'c-ls)^2 - 2(kc-ls)(k'c-ls)\exp\{-D_2 t/\sigma_2{}^2\}]\right\} \quad \text{(A13)}$$

For $t = 0$ it follows, after some algebra, that $C_{\mu\nu}(0) = P_2(\mathbf{e}_\mu\cdot\mathbf{e}_\nu)$. For long times, $C_{\mu\nu}(t)\mathrm{e}^{6Dt}$ reaches a plateau value, given by the order parameter $S_{\mu\nu}{}^2$,

$$\lim_{t\to\infty} C_{\mu\nu}(t)\mathrm{e}^{6Dt} = S_{\mu\nu}{}^2 = (4\pi/5)\sum_{k,k',l=-2}^{2} \mathrm{d}^{(2)}_{kl}(\pi-\beta)\, \mathrm{d}^{(2)}_{k'l}(\pi-\beta)\, Y_{2k}(\Omega^{\mathrm{ring}}_{\mu}) \times Y_{2k'}{}^*(\Omega^{\mathrm{ring}}_{\nu})\, F_{kl}F_{k'l} \quad \text{(A14)}$$

where $F_{kl} = \exp\{-(1/2)[l^2\sigma_{\chi_1}{}^2 + k^2\sigma_{\chi_2}{}^2 + 2lk\sigma_{\chi_1}\sigma_{\chi_2}r\}$ and the correlation coefficient r has been defined in eq A4. Spin pairs which experience motions about both χ_1 and χ_2 yield order parameters $S_{\mu\nu}{}^2$ which carry combined information on $\sigma_1{}^2$, $\sigma_2{}^2$, and r. For a sufficiently large number of internuclear vectors probing different orientations, determination of all three parameters σ_{χ_1}, σ_{χ_2}, and r using eq A14 is possible, provided that $\sigma_{\chi_1}{}^2 \neq \sigma_{\chi_2}{}^2$.

For C−H spin pairs which experience only motion about χ_1, such as C^β−H^β pairs, eq A14 reduces to the one-dimensional GAF model[25]

$$S^2 = 1 - 3\cos^2\theta\{\cos^2\theta(1-\mathrm{e}^{-\sigma_{\chi_1}{}^2}) + (1/4)\sin^2\theta(1-\mathrm{e}^{-4\sigma_{\chi_1}{}^2})\} \quad \text{(A15)}$$

Adding Multiple Lattice Site Jumps in χ_1 and χ_2. Exchange between rotamers in χ_1 and χ_2 can be included in a straightforward way if one assumes that such motion is statistically independent of the Gaussian fluctuations and that the harmonic potentials are identical in each rotamer. For this purpose we introduce average χ values for the rotameric conformations μ of χ_1 and χ_2 and denote them by $\bar\chi_1(u)$ and $\bar\chi_2(u)$, respectively. It follows that

$$C_{\mu\nu}(t) = \sum_{k,k',l=-2}^{2} \langle \mathrm{e}^{ik\chi_2(t)+il\chi_1(t)}\mathrm{e}^{-ik'\chi_2(0)-il\chi_1(0)}\rangle_{\mathrm{GAF}} \times \langle \mathrm{e}^{ik\bar\chi_2(t)+il\bar\chi_1(t)}\mathrm{e}^{-ik'\bar\chi_2(0)-il\bar\chi_1(0)}\rangle_{\mathrm{jump}} (4\pi/5)\mathrm{e}^{-6Dt}\, \mathrm{d}^{(2)}_{kl}(\pi-\beta) \times \mathrm{d}^{(2)}_{k'l}(\pi-\beta)\, Y_{2k}(\Omega^{\mathrm{ring}}_{\mu})\, Y_{2k'}{}^*(\Omega^{\mathrm{ring}}_{\nu}) \quad \text{(A16)}$$

The first average is of the type in eq A13 while the second average includes averaging over the different rotameric states. From the standard treatment of the lattice jump model (see, e.g., ref 43), it follows that the conditional probabilities $P(w,t|u,0)$, which the system occupies at time t state w if it was at time 0 in state u, obey a master equation

$$\dot{\mathbf{P}} = \mathbf{KP} \quad \text{with} \quad P(w,0|u,0) = \delta_{uw} \quad \text{(A17)}$$

where the matrix element $[\mathbf{K}]_{wu}$ is the transition rate constant between sites u and w. Equation A17 has the formal solution

$$P(w,t|u,0) = [\mathrm{e}^{\mathbf{K}t}]_{wu} \quad \text{(A18)}$$

In thermal equilibrium all sites are populated with Boltzmann populations, $p(w) = \lim_{t\to\infty} P(w,t|u,0)$. Insertion of eq A18 into eq A16 yields

$$C_{\mu\nu}(t) = \frac{4\pi}{5}\mathrm{e}^{-6Dt}\sum_{k,k',l=-2}^{2}\sum_{u,w} \mathrm{d}^{(2)}_{kl}(\pi-\beta)\, \mathrm{d}^{(2)}_{k'l}(\pi-\beta) \times Y_{2k}(\Omega^{\mathrm{ring}}_{\mu})\, Y_{2k'}{}^*(\Omega^{\mathrm{ring}}_{\nu})\, p(u) \times [\mathrm{e}^{\mathbf{K}t}]_{wu}\mathrm{e}^{ik\bar\chi_2(w)+il\bar\chi_1(w)-ik'\bar\chi_2(u)-il\bar\chi_1(u)} \exp\left\{-\frac{1}{2}\sigma_1{}^2[(1c+ks)^2 + (lc+k's)^2 - 2(lc+ks)(lc+k's)\exp\{-D_1 t/\sigma_1{}^2\}]\right\} \times \exp\left\{-\frac{1}{2}\sigma_2{}^2[(kc-ls)^2+(k'c-ls)^2 - 2(kc-ls)(k'c-ls)\exp\{-D_2 t/\sigma_2{}^2\}]\right\} \quad \text{(A19)}$$

In case the rotameric exchange processes of χ_1 and χ_2 are independent, they can be described by two master equations with kinetic matrices $\mathbf{K}_1$ and $\mathbf{K}_2$, respectively. The average of eq A16 can then be split into an average over χ_1 rotamers a, b = 1, ..., M and an average over χ_2 rotamers u, w = 1, ..., N:

$$\langle \mathrm{e}^{il\bar\chi_1(t)-il\bar\chi_1(0)}\mathrm{e}^{ik\bar\chi_2(t)-ik'\bar\chi_2(0)}\rangle_{\mathrm{jump}} = \langle \mathrm{e}^{il\bar\chi_1(t)-il\bar\chi_1(0)}\rangle_{\mathrm{jump},\chi_1}\langle \mathrm{e}^{ik\bar\chi_2(t)-ik'\bar\chi_2(0)}\rangle_{\mathrm{jump},\chi_2} \quad \text{(A20)}$$

where

$$\langle \mathrm{e}^{il\bar\chi_1(t)-il\bar\chi_1(0)}\rangle_{\mathrm{jump},\chi_1} = \sum_{a,b} p_1(a)[\mathrm{e}^{\mathbf{K}_1 t}]_{ba}\mathrm{e}^{il\bar\chi_1(b)-il\bar\chi_1(a)} \quad \text{(A21)}$$

$$\langle \mathrm{e}^{il\bar\chi_2(t)-ik'\bar\chi_2(0)}\rangle_{\mathrm{jump},\chi_2} = \sum_{u,w} p_2(u)[\mathrm{e}^{\mathbf{K}_2 t}]_{wu}\mathrm{e}^{ik\bar\chi_2(w)-ik'\bar\chi_2(u)} \quad \text{(A22)}$$

This separation has been used together with $r = 0$ ($c = 1$, $s = 0$) for the analysis of the NMR relaxation data calculated from the LD trajectory:

$$C_{\mu\nu}(t) = \frac{4\pi}{5} e^{-6Dt} \sum_{k,k',l=-2}^{2} \sum_{a,b} \sum_{u,w} d_{kl}^{(2)}(\pi-\beta)\, d_{k'l}^{(2)}(\pi-\beta) \times Y_{2k}(\Omega_\mu^{\mathrm{ring}})\, Y_{2k'}{}^*(\Omega_\nu^{\mathrm{ring}})\, p(a)[e^{\mathbf{K}_1 t}]_{ba} e^{il\bar{\gamma}_1(b)-il\bar{\gamma}_1(a)} \times p(u)[e^{\mathbf{K}_2 t}]_{wu} e^{ik\bar{\gamma}_2(w)-ik'\bar{\gamma}_2(u)} \exp\left\{-\frac{1}{2}\sigma_{\chi_1}{}^2 l^2 (1 - \exp\{-D_1 t/\sigma_{\chi_1}{}^2\})\right\} \exp\left\{-\frac{1}{2}\sigma_{\chi_2}{}^2 (k^2 + k'^2 - 2kk' \times \exp\{-D_2 t/\sigma_{\chi_2}{}^2\})\right\} \quad \text{(A23)}$$

The power spectral density function $J_{\mu\nu}(\omega)$ which enters the relaxation equations is obtained by Fourier transformation of $C_{\mu\nu}(t)$. The Fourier transform of the terms of type

$$f(t) = \exp(A + B \exp(-D_\alpha t/\sigma_\alpha{}^2)) \quad \text{(A24)}$$

contained in eq A23, can be calculated analytically by using a Taylor series expansion of the outer exponential function,

$$f(t) = \lim_{N\to\infty} \sum_{n=0}^{N} \frac{(A + B \exp(-D_\alpha t/\sigma_\alpha{}^2))^n}{n!} = \lim_{N\to\infty} \sum_{n=0}^{N} \sum_{m=0}^{N} \binom{n}{m} \frac{A^{n-m} B^m \exp(-mD_\alpha t/\sigma_\alpha{}^2)}{n!} \quad \text{(A25)}$$

where good convergence is usually obtained already for small N. The Fourier transform of $f(t)$ can then be represented as a sum of Lorentzians of the form $2\sigma_\alpha{}^2\{mD_\alpha(1 + (\omega\sigma_\alpha{}^2/mD_\alpha)^2)\}^{-1}$.

The autospectral density function $J_\mu(\omega) \equiv J_{\mu\mu}(\omega)$ can be used to evaluate the standard expressions for longitudinal dipolar relaxation of a ^{13}C spin attached to N protons:[1]

$$\left(\frac{1}{T_1}\right)_D = N\frac{1}{20}\left(\frac{\mu_0}{4\pi}\right)^2\left(\frac{h}{2\pi}\right)^2 \gamma_C{}^2\gamma_H{}^2\langle r_{CH}{}^{-3}\rangle^2\{3J_\mu(\omega_C) + J_\mu(\omega_C-\omega_H) + 6J_\mu(\omega_C+\omega_H)\} \quad \text{(A26)}$$

where γ_C and γ_H are the gyromagnetic ratios of the nuclei and ω_C and ω_H their Larmor frequencies, respectively; h is Planck's constant, μ_0 is the magnetic field constant, and r_{CH} is the internuclear distance.

The corresponding heteronuclear steady-state $\{^1H\}^{13}C$ NOE η is

$$\eta = 1 + \frac{\gamma_H}{\gamma_C}\left[N\frac{1}{20}\left(\frac{\mu_0}{4\pi}\right)^2\left(\frac{h}{2\pi}\right)^2 \gamma_C{}^2\gamma_H{}^2\langle r_{CH}{}^{-3}\rangle^2\{6J_\mu(\omega_C+\omega_H) - J_\mu(\omega_C-\omega_H)\}/T_1{}^{-1}\right] \quad \text{(A27)}$$

where T_1 is the total ^{13}C T_1 relaxation time including the CSA contribution.

For an axially-symmetric CSA tensor, one can use the standard formula

$$\left(\frac{1}{T_1}\right)_{CSA} = \frac{1}{15}(\sigma_{\parallel} - \sigma_{\perp})^2 \omega_C{}^2 J_\mu(\omega_C) \quad \text{(A28)}$$

where $\sigma_{\parallel}$ and $\sigma_{\perp}$ are the chemical shielding tensor components parallel and perpendicular to the symmetry axis defined by $\Omega_\mu^{\mathrm{ring}}$.

For a non-axially-symmetric CSA tensor the situation is more complicated. We use here the fact that any non-axially-symmetric tensor can be described as a superposition of two axially-symmetric, orthogonal tensors. In the CSA principal axis system σ (with $Tr\{\sigma\} = 0$) is[44]

$$\sigma = \begin{bmatrix} \sigma_{xx} & 0 & 0 \\ 0 & \sigma_{yy} & 0 \\ 0 & 0 & \sigma_{zz} \end{bmatrix} = \frac{1}{3}\sigma_x \begin{bmatrix} 2 & 0 & 0 \\ 0 & -1 & 0 \\ 0 & 0 & -1 \end{bmatrix} + \frac{1}{3}\sigma_y \begin{bmatrix} -1 & 0 & 0 \\ 0 & 2 & 0 \\ 0 & 0 & -1 \end{bmatrix} \quad \text{(A29)}$$

where $\sigma_x = \sigma_{xx} - \sigma_{zz}$ and $\sigma_y = \sigma_{yy} - \sigma_{zz}$. CSA relaxation can thus be described as the sum of two autocorrelated CSA relaxation terms and one cross-correlated CSA relaxation term,

$$\left(\frac{1}{T_1}\right)_{CSA} = \frac{1}{15}\omega_C{}^2\{\sigma_x{}^2 J_{xx}(\omega_C) + \sigma_y{}^2 J_{yy}(\omega_C) + 2\sigma_x\sigma_y J_{xy}(\omega_C)\} \quad \text{(A30)}$$

where $J_{xx}(\omega)$ indicates that $\Omega_\mu^{\mathrm{ring}} = \Omega_\nu^{\mathrm{ring}}$ in eq A19 points along the x axis of the CSA tensor, and correspondingly in $J_{yy}(\omega)$, $\Omega_\mu^{\mathrm{ring}} = \Omega_\nu^{\mathrm{ring}}$ points along the y axis of the CSA tensor. For the cross-correlation term $J_{xy}(\omega)$, $\Omega_\mu^{\mathrm{ring}}$ is parallel to the x axis while $\Omega_\nu^{\mathrm{ring}}$ is parallel to the y axis. The total $T_1{}^{-1}$, which enters also eq A27 for the NOE η, is then $T_1{}^{-1} = (T_1{}^{-1})_D + (T_1{}^{-1})_{CSA}$. It is noted here that the CSA treatment used in eq 4 of ref 24 is correct only for an axially-symmetric CSA tensor interaction. For the general case of a non-axially-symmetric CSA tensor, eq A30 has to be used.

JA9636505